Tunable-angle wedge transducer for improved acoustophoretic control in a microfluidic chip

I Iranmanesh[1,3]**, R Barnkob**[2]**, H Bruus**[2] **and M Wiklund**[1]

[1] Department of Applied Physics, Royal Institute of Technology, AlbaNova University Center,
SE-106 91 Stockholm, Sweden
[2] Department of Physics, Technical University of Denmark, DTU Physics Building 309,
DK-2800 Kongens Lyngby, Denmark

E-mail: ida.iranmanesh@biox.kth.se

Abstract

We present a tunable-angle wedge ultrasound transducer for improved control of microparticle acoustophoresis in a microfluidic chip. The transducer is investigated by analyzing the pattern of aligned particles and induced acoustic energy density while varying the transducer geometry, transducer coupling angle, and transducer actuation method (single-frequency actuation or frequency-modulation actuation). The energy-density analysis is based on measuring the transmitted light intensity through a microfluidic channel filled with a suspension of 5 μm diameter beads and the results with the tunable-angle transducer are compared with the results from actuation by a standard planar transducer in order to decouple the influence from change in coupling angle and change in transducer geometry. We find in this work that the transducer coupling angle is the more important parameter compared to the concomitant change in geometry and that the coupling angle may be used as an additional tuning parameter for improved acoustophoretic control with single-frequency actuation. Further, we find that frequency-modulation actuation is suitable for diminishing such tuning effects and that it is a robust method to produce uniform particle patterns with average acoustic energy densities comparable to those obtained using single-frequency actuation.

(Some figures may appear in colour only in the online journal)

1. Introduction

Ultrasonic actuation of microfluidic chips can be used for acoustofluidic manipulation of suspended particles, cells or the fluid medium [1]. Many different techniques for the acoustic coupling into a fluid channel have been reported, including the use of bulk acoustic waves (BAWs) [2], surface acoustic waves (SAWs) [3] and plate waves [4]. In our group, we have previously used a technique based on a coupling wedge for BAW excitation [5] combined with frequency-modulation (FM) actuation [6]. However, it is not fully understood how this coupling mechanism works and how the transducer geometry and coupling angle influence the obtained acoustic radiation force field on particles inside the fluid channel, nor has the obtained acoustic energy density been evaluated when using FM actuation rather than using single-frequency (SF) actuation. Thus, two main questions motivate this work: (i) what are the design criteria when using a wedge transducer for acoustophoresis, and (ii): does FM actuation compromise the efficiency of acoustophoresis relative SF actuation when using a wedge transducer?

The traditional design of a transducer–chip system for BAW acoustophoresis is to attach a planar transducer to a planar microchip, and then to match either the channel width (orthogonal coupling) [7] or height (parallel coupling) [8] with a multiple of half the acoustic wavelength. In this way, a standing wave is formed in the channel and particles can be driven to the pressure nodes of the standing wave by

---

[3] Author to whom any correspondence should be addressed.

1
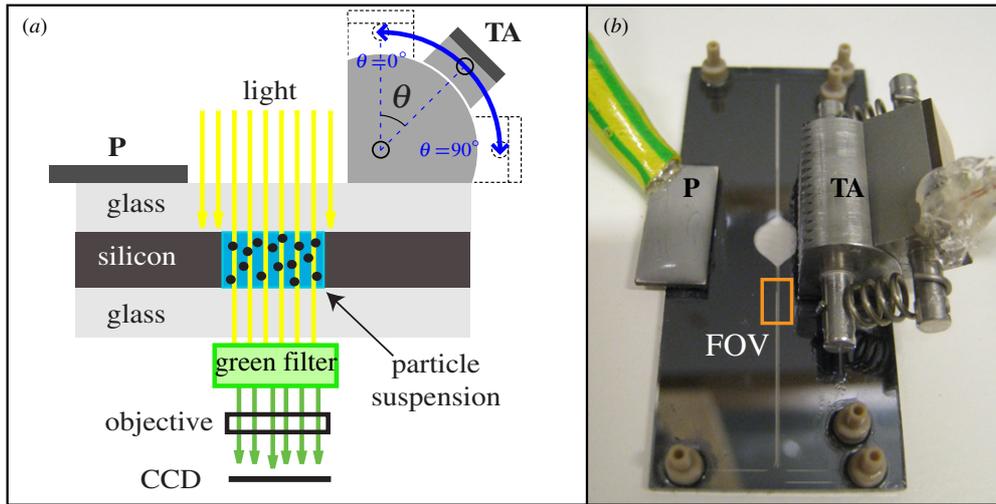
Figure 1. (*a*): Schematic cross-section view of the setup (not to scale). The chip consists of a silicon layer (dark gray) sandwiched in between two glass layers (light gray). It is actuated by either a planar (P) transducer or tunable-angle (TA) transducer. The angle θ of the TA transducer can be adjusted continuously between 0 and 90°. Light from the microscope condenser (yellow arrows) passes through the transparent microchannel containing a particle suspension. The particle motion is recorded by the CCD camera using an inverted microscope with a green filter. (*b*): Photo of the setup consisting of the planar (P) and TA transducers mounted on the acoustophoresis chip. The motion of the particles due to acoustophoresis is observed in the field of view of the microscope objective, which is marked with the orange rectangle (FOV). The microchannel is 328 μm wide and 110 μm deep. The large rounded chamber in the middle of the chip was not used in this study, but has been investigated elsewhere [21].

the primary radiation force [9]. Independent on the coupling method, BAW acoustophoresis applied to a simple straight microchannel of constant cross section is difficult to drive in a pure one-dimensional (1D) resonance mode; instead particles are collected in bands of complex 3D shapes. Typically, the bands of aligned particles have a fragmented and/or twisted shape [10]. However, such shapes are generally not a problem as long as the device is operated in flow-through-mode. This is the case in most acoustophoretic applications which are based on the net effect of translating the particles into a well-defined fluid streamline after the active part of the microchannel. However, for more accurate flow-based acoustophoresis [11], or for acoustophoresis not based on a continuous fluid flow [6, 12], the complex 3D shapes of manipulated particles may be problematic. This is particularly important in applications of acoustic manipulation of individual cells or particles [12, 13]. In addition to fine-tuning the actuation frequency, methods for controlling the non-ideal shapes of manipulated particles are, for example, to employ pulsed actuation [14] or FM actuation [6, 12, 13, 15]. The latter technique (FM) is developed in our lab and based on averaging the shapes of particles from several single frequencies. Although proven useful in cell manipulation applications [13], FM actuation has never been quantified and compared with standard SF actuation.

Different wedge transducer designs for acoustophoresis were first studied by Manneberg *et al* [5], who concluded that a 30° wedge transducer was superior a planar transducer in their particular setup. However, a limitation in the work of Manneberg *et al* was that because they used different transducers, the influence of different geometries, sizes and positions of the wedges on the observed resonances could not be resolved from the influence of different coupling angles. For that reason, in this work we study a novel tunable-angle (TA) wedge transducer where the wedge angle can be continuously

tuned between 0° and 90° on the same transducer (cf figure 1). Furthermore, we use a planar (P) reference transducer of more traditional design (i.e. with standard orthogonal coupling, corresponding to 0° in figure 1) for investigating the effect of changing the coupling angle when the TA transducer is turned off. This allows for analysis of the influence of both the transducer geometry (passive TA transducer) and the coupling angle (active TA transducer) of the wedge transducer, when at any given time only one of the actuators (TA or P) is active. We investigate the pattern of manipulated 5 μm diameter beads in the channel, for which the radiation force dominates over the streaming-induced drag force [16, 17], and we quantify the acoustic energy densities in different parts of the channel for the different actuation configurations by the use of a recently reported light-intensity method [18]. We show that the wedge coupling angle of the TA transducer has a significant influence on the obtained particle pattern and acoustic energy density, and that when properly implemented, the FM method is not only more robust but can also lead to average acoustic energy densities comparable to those obtained by standard SF actuation. We also show that for SF actuation, the wedge angle can be used as an additional tuning parameter (besides frequency and temperature) for controlling the shape and magnitude of the acoustic radiation force field in the channel.

2. Theoretical background

In this section we discuss acoustic resonances in a microfluidic channel (section 2.1), the acoustic radiation force acting on a suspended particle (section 2.2), and the light-intensity model used for estimating the energy density in the fluid channel (section 2.3).

2.1. Acoustic resonances in a microchannel

The microfluidic chip of interest for this study is a glass/silicon/glass structure with a microchannel of rectangular cross section filled with a liquid. If the purpose is to establish a half-wave resonance mode across the channel width ($\lambda = 2w$), the simple 1D approximation yields a resonance frequency f and acoustic pressure amplitude p as [19]:

$$f = \frac{c_0}{2w} \quad \text{and} \quad p(y) = p_a \cos(k_y y). \quad (1)$$

Here, c_0 is the sound velocity in the fluid, w is the channel width, y is the coordinate along the channel width w, and $k_y = 2\pi/\lambda$ is the 1D wavenumber (where λ is the wavelength in the fluid). Equation (1) is useful when predicting the local pressure field in the channel and forms the basis in the method for measuring the acoustic energy density (see section 2.3). However, it is well known that acoustic resonances in microchannels are not purely 1D. In particular, many groups have observed and/or quantified variations in the pressure field along the channel length [5, 6, 10, 16, 19]. Typically, a fragmented and/or curved resonance pattern is obtained in channels with length l larger or much larger than the wavelength, λ. Another consequence of half-wave resonances in channels with $w \ll l$ is the relatively small frequency step Δf_{res} between neighboring resonances. For example, Δf_{res} is of the order of 10 kHz in microchannels of length a few centimeters when operated at a half-wave mode of a few megahertz [16, 19]. As a result, a half-wave acoustophoretic chip can be driven at many different frequencies around the nominal (1D) half-wave resonance frequency described by equation (1). This is the basis of our employed FM method [6, 12], i.e., to produce a time-averaged resonance that is the average of several SF resonances within a suitable bandwidth around the nominal 1D resonance. According to our experience [6], this bandwidth should preferably be one order of magnitude larger than Δf_{res}, i.e. at least 100 kHz which results in a resonance that is the average of at least ten SF resonances.

2.2. The acoustic radiation force on a single particle

If we assume a local 1D pressure field according to equation (1) (i.e. not considering any x-dependence along the channel), the acoustic radiation force on a single particle with radius $a \ll \lambda$ can be estimated by using the following formula first derived by Yosioka and Kawasima [20]:

$$F_y^{rad} = 4\pi \Phi k_y a^3 E_{ac} \sin(2k_y y), \quad (2a)$$

$$\Phi = \frac{1}{3} \left[\frac{5\tilde{\rho} - 2}{2\tilde{\rho} + 1} - \tilde{\kappa} \right]. \quad (2b)$$

Here, Φ is the acoustic contrast factor where $\tilde{\rho} = \rho_P/\rho_0$ and $\tilde{\kappa} = \kappa_p/\kappa_0$ is the density and compressibility ratios between the particle (index 'p') and the fluid medium (index '0'), respectively. The relationship between the acoustic energy density, E_{ac}, and the acoustic pressure amplitude, p_a is important for the measurements in this paper:

$$E_{ac} = \frac{p_a^2}{4\rho_0 c_0^2}. \quad (3)$$

2.3. Light-intensity model for estimating the acoustic energy density

The 1D model described in equations (1)–(3) forms the basis for a recently reported light-intensity model to be used for estimation of the acoustic energy density in the fluid channel. The method is described in detail in [18], but a brief summary follows here.

The method is based on the sum of the light intensity I_α obtained from each pixel in an image of a segment of the microchannel, but only from a certain interrogation area of relative width α (relative the channel width w) [18]. This interrogation area is defined as the entire fluid channel except the final band of particles agglomerated in the pressure node of the standing wave. This band has the relative width $1-\alpha$ and is dependent on the particle concentration, and must therefore be tuned manually for a certain experimental condition. Thus, ideally, I_α should converge at time $t = \infty$ to a maximum value $I_\alpha(\infty)$ where no particles are left in the interrogation area to shade the transmitted light. In this way, the relative light intensity $I_\alpha(t)/I_\alpha(\infty)$ at time t can be defined as:

$$I_\alpha(t)/I_\alpha(\infty) = 1 - (2R/\alpha\pi) \arctan[\tan(\pi\alpha/2)\,e^{-t/t^*}], \quad (4)$$

where $R = 1 - I_\alpha(0)/I_\alpha(\infty)$ is the relative intensity reduction at $t = 0$, defined by the initial and final light intensities, $I_\alpha(0)$ and $I_\alpha(\infty)$, respectively. Here the characteristic time t^* is defined as

$$t^* = \frac{3\eta}{4\Phi(\pi a/w)^2} \frac{1}{E_{ac}}, \quad (5)$$

where η is the fluid viscosity. Thus, the acoustic energy density E_{ac} in equation (5) can be used as a fitting parameter and can easily be translated to acoustic pressure amplitude p_a via equation (3).

When comparing the light-intensity method with other available methods for indirect measurements of the energy density or pressure amplitude, the main advantage of our method is that it is applicable to particle suspensions of higher concentrations than what can be used with, e.g., particle image velocimetry (PIV) analysis. Furthermore, the method is also applicable to images with limited resolution. For example, single particles do not need to be clearly resolved, and it is not so important that the particles are in the focal plane of the microscope. This allows for the use of microscope objectives providing larger field of views than possible with PIV analysis. In the experiments described below, we have used the light-intensity model on image subsections along the channel length $x \approx 1.3$ mm from a single video clip, in order to measure the spatial distribution of acoustic energy density for different modes of actuation.

3. Experimental arrangements

3.1. Experimental setup

Microfluidic chip. We used a microfabricated glass-silicon-glass chip (GeSim, Dresden, Germany) with layer thickness of 0.20/0.11/1.10 mm (bottom glass/silicon/upper glass), respectively, as shown in figure 1. This chip is described in more detail in [21]. In this work we studied the part of the

microchannel marked by the orange rectangle in figure 1(*b*). In this part of the channel, the cross section was rectangular with width $w = 328\ \mu$m and height $w = 110\ \mu$m. The channel width is chosen to match the half-wave condition $\lambda/2 = w$ or $f = c/(2w)$ across the width corresponding to a resonance frequency around 2.2 MHz (cf equation (1)).

Transducers. Two kinds of transducers were built and used for the experiments: a TA transducer and a P transducer (see figure 1). The TA transducer is made of an aluminum wedge which is connected by two springs to a quarter-cylindrical aluminum base plate. A small volume (approx. 1 μL) of microscope immersion oil was used to facilitate the movement of the upper wedge on the base plate and for acoustic coupling. The angle θ of the TA transducer can be tuned continuously between 0° and 90°. Here, we define θ as the angle between the normal to the chip surface and the (thickness-mode) vibration direction of the piezo crystal (cf figure 1). However, note that this definition means that the angle between the piezo vibration and the intended radiation force in the channel is $90° - \theta$. The specific angles investigated in this work were selected from 0° to 90° in steps of 15°, and the corresponding wedge positions were marked on the base plate of the wedge. The P transducer was made with a thin layer of epoxy backing in order to be used as a reference transducer in some of the experiments. The resonance peaks (center frequency and bandwidth) of the transducers were identified by scanning their electrical admittance with an impedance analyzer (Z-Check 16777 k, SinePhase, Austria). Both transducers were designed to be resonant around 2 MHz. The amount of backing layer of the P transducer was selected to achieve a bandwidth similar to the one of the TA transducer (approx. 250 kHz for both the P and TA transducers). Furthermore, the SFs and center frequency of the FMs used was selected from the resonance peaks of the admittance curves. Since changing the angle of the TA transducer had little effect on the admittance, we chose to use the same SF and center frequency of FM when changing the TA transducer angle in the experiment.

Particle suspension. The fluid suspension consisted of 5 μm diameter polyamide beads (Orgasol Powders, Arkema, France) diluted in Milli-Q water (with 0.01% Tween20). Using a Coulter counter, the final concentration of the suspension was approx 10^9 beads per mL and the calibrated bead diameter was $(4.5 \pm 0.7)\ \mu$m.

Temperature measurements. The temperature on the transducer surfaces was monitored with a Teflon insulated T-type micro thermocouple (IT-21, Physitemp Instruments, USA) connected to a data logging unit (Dostmann Electronic GmbH P655-LOG, Germany). During all experiments, the temperature variations were less than 1 °C, which ensures resonance frequency shifts of less than 0.1 kHz [16].

Microscopy. An inverted microscope (Axiovert 40, Zeiss, Germany) was used to image the microchannel with a 10 × /0.25 N.A. objective (A-Plan, Zeiss, Germany). A closed circuit diagram (CCD) camera (AxioCam HSC, Zeiss, Germany) was used to record video clips with a frame rate of 5 fps, and a set of images were extracted from the video clips by the use of Axio Vision Rel.4.8 software. The rectangular field of view (FOV) of the channel had the dimensions of $328 \times 1225\ \mu$m^2 or 168×628 pixels, which means that the width of each pixel is approximately 2 μm.

3.2. Experimental procedure

Microbead-acoustophoresis with no flow. In all our experiments, the polyamide microbead suspension was injected into the microchannel using a plastic syringe, and the suspension flow was stopped using microvalves connected to the microchannel. When the fluid motion settled, the transducers were activated (one at a time) and the acoustophoretic motion of the particles was recorded by starting the video just before a transducer was turned on. The duration of the recorded video was typically 30 s to ensure that the acoustophoresis had reached a near-steady state. For the TA transducer, the experiments were performed with SF actuation around 2.19 MHz as well as with FM actuation (saw-tooth sweeps with center frequency of 2.19 MHz, bandwidth 100 kHz, and modulation rate of 1 kHz). For the P transducer the procedure was the same but the center frequency was in this case 2.00 MHz. The SF for each transducer (TA and P) was selected from the maximum (real-part) admittance measured by impedance spectroscopy when the transducers were attached to the chip. For FM actuation, the optimal SF was used as center frequency for both transducers (TA and P). The choice of FM actuation bandwidth (100 kHz) was based on a trade-off between transducer bandwidth (∼250 kHz) and frequency step between neighboring resonances (Δf_{res}, cf section 2.1). The chosen SFs of this investigation were the most efficient SFs within the FM bandwidth, which was confirmed by impedance analysis and visual inspection of bead motion in the channel. Both transducers were driven at 20 V peak-to-peak.

Acoustic energy density measurement. Based on the light-intensity method described in section 2.3, the acoustic energy density was estimated along the specified rectangular field of view (FOV in figure 1(*b*)) of the channel. We used $\alpha = 0.8$ (cf equations (4) and (5)), which means that we excluded $1 - \alpha = 20\%$ of the central part of the channel (where the aggregated line of particles is expected to end up) when integrating the light detected by the CCD. We measured the acoustic energy density for the polyamide beads having radius $a = (2.25 \pm 0.35)\ \mu$m over a channel segment of length 1.2 mm. However, the variation in radius $\Delta a = \pm\ 0.35\ \mu$m (about 15%) was not taken into account when fitting the data to the model.

Dependence of the acoustic energy density on the coupling angle. An experimental series was performed when the TA transducer was turned on and the angle of incidence tuned between 0° and 90° in steps of 15°, while the P transducer was turned off. The light-intensity method was employed for estimating the dependence of the energy density on the coupling angle when driving the system with the TA transducer with SF actuation as well as for FM actuation.

Dependence of the acoustic energy density on the transducer geometry. In these experiments the P transducer was the active one, while the TA transducer was turned off. Then, during the P-transducer operation, we changed the angle on the passive TA transducer. In this way, we could measure the
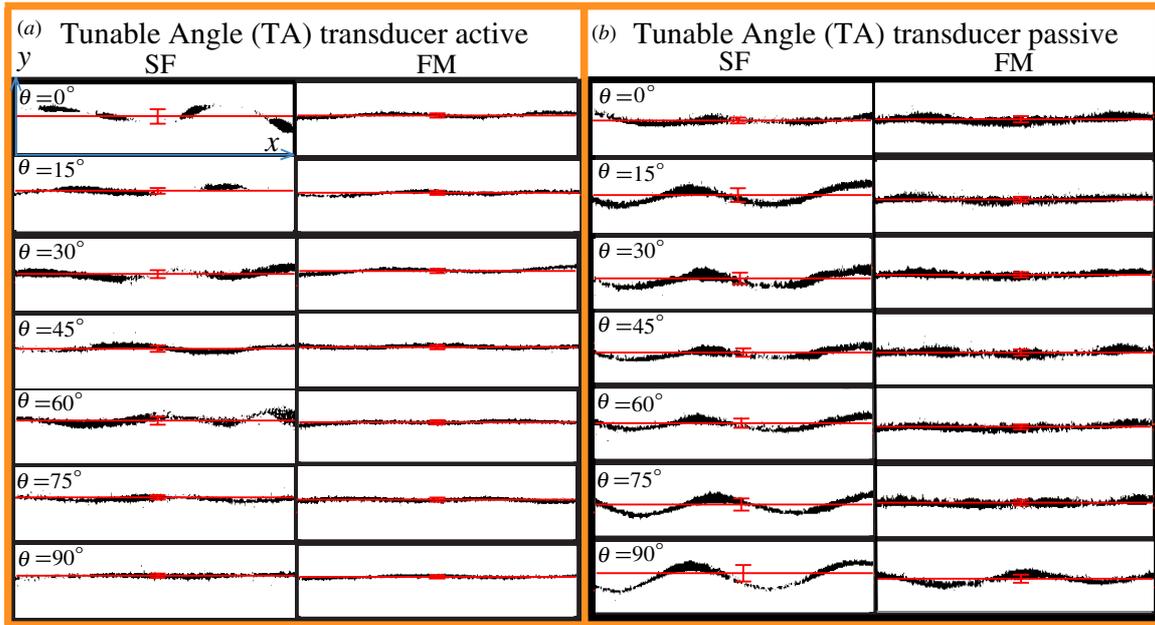
Figure 2. Acoustophoresis patterns of 5 μm diameter particles after 30 s of actuation as a function of the angle on the active (*a*) and passive (*b*) TA transducer. (*a*): the TA transducer active (P transducer passive), and (*b*): the TA transducer passive (P transducer active). The measurements were performed at single frequency (SF, left column) and frequency-modulation (FM, right column) actuation of each active transducer, TA in (*a*) and P in (*b*). In (*b*), the TA transducer is only used passively for changing the geometry of the device. The error bars mark the standard deviation (Δ) of the pattern from a straight line along x around its mean position (solid red lines).

dependence of the acoustic energy density on the change in TA transducer geometry while keeping the coupling angle constant on the active transducer (fixed at $0°$ for the P transducer). The reason is by changing the angle of the TA transducer, not only the coupling angle changes but also the whole geometry of the system including the center of mass. This may in turn change the resonance characteristics of the device. The investigated angles on the passive TA transducer were the same as in the experiment where the TA transducer was active.

Reproducibility tests. The reproducibility of the results when changing the angle of the TA transducer was investigated by mounting and demounting the TA transducer on the microchip and then repeating the experiment. For each repetition, the same amount of immersion oil (1 μL) was used between the two parts of the TA transducer.

4. Results and discussion

4.1. Acoustophoresis particle patterns

The pattern of particles after 30 s of acoustophoresis was investigated as a function of the coupling angle of the TA transducer. We studied the pattern when actuating the chip with either the TA transducer (figure 2(*a*)) or the P transducer (figure 2(*b*)). The experiment was performed for both SF actuation as well as for FM actuation. For the range of angles $0° \leqslant \theta \leqslant 90°$ of the TA transducer, we analyzed the deviation of the final pattern from an ideal straight line by measuring the position $y(x_j)$ of the focusing pattern at N selected axial positions x_j and then calculating the variance $\Delta^2 = (1/N) \sum_{j=1}^{N} [y(x_j) - y_c]^2$, see figure 3. Here, y_c is the
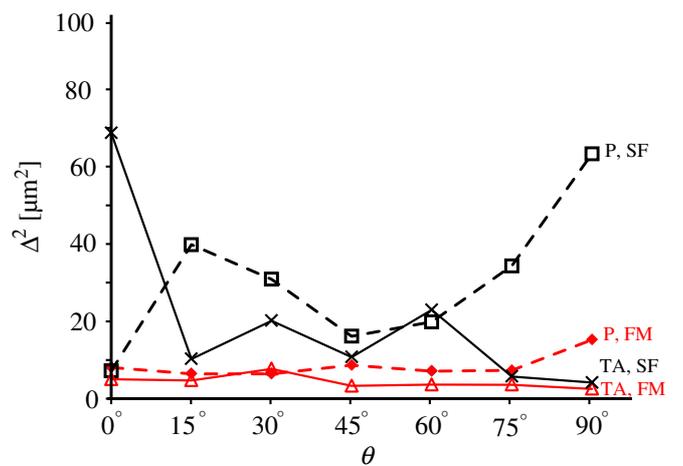
Figure 3. The variances Δ^2 from an ideal straight line of the patterns in figure 2 plotted as a function of the angle for planar (P) and TA transducer for both SF and FM actuation modes.

position of a straight line chosen to minimize Δ^2. In figure 2, the solid and dashed lines show $y_c \pm \Delta$ as a function of the angle, θ, when actuating the chip with either the TA transducer (figure 2(*a*)), or the P transducer (figure 2(*b*)), and for both combinations of actuation: SF and FM. This calculation was performed after processing the images in ImageJ and Matlab. As can be clearly seen in figures 2 and 3, the spatial variations of the particle patterns in the focusing direction (*y*) are less for FM actuation than for SF actuation for all investigated angles. For example, when averaging the variances in figure 3 over all angles we get $\Delta_{FM}^2 / \Delta_{SF}^2 = 0.29$ for the P transducer and 0.18 for the TA transducer. Thus, the smallest variances are
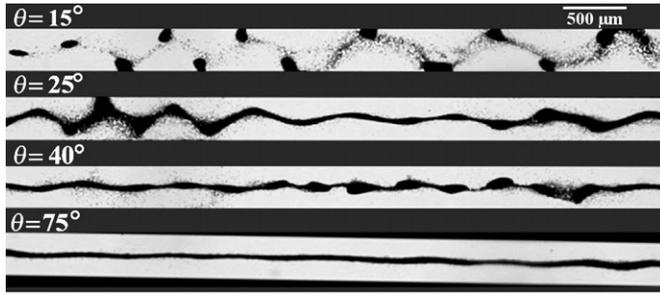
Figure 4. Steady-state acoustophoresis patterns of 5 μm diameter particles after 10 min of SF actuation with the TA transducer for 4 different angles.

obtained for FM actuation of the TA transducer, suggesting that this method is the most suitable for obtaining uniform acoustophoresis along the channel. Furthermore, not only the variance but the shapes of the patterns vary with angle θ. For example, in figure 2 we see that for SF actuation the positions along x of peaks and valleys in the patterns also changes with θ. Since this is obtained for not only active TA transducer but also for active P transducer, there is a noticeable acoustophoretic effect in changing the device geometry (i.e. changing θ of the passive TA transducer) although both the fluid channel and the active P transducer are fixed (see figure 2(a)). We also notice that we may produce relatively uniform particle patterns with SF actuation for some coupling angles (e.g., $\theta \geqslant 75°$, TA active). This is even more evident when studying the final pattern after long actuation times ($\sim$10 min), see figure 4. In this experiment, the pattern for the largest angle is similar to the uniform (1D) pattern of FM actuation, while the other angles produce complex 3D patterns characterized by curved and/or fragmented particle aggregates along the channel. However, this pattern is not only dependent on the resonance mode in the channel, but also on particle-particle interactions making these patterns very difficult to model and predict. In summary, we may conclude that the coupling angle of the TA transducer is important for controlling the acoustophoresis particle pattern (in particular when the TA transducer is active), and that it is possible to tune the device into a near-1D resonant mode in the fluid channel for SF actuation. However, we also conclude that FM actuation reduces the need for this fine-tuning and provides higher robustness in the acoustophoresis operation for any coupling angle and device geometry.

After the variance analysis of the particle patterns along x, we used the light-intensity method (cf section 2.3) for quantifying the acoustic energy density $E_{ac}(\theta)$ obtained for the experiments in figure 2. The result is shown in figures 5(a) and (b), where the relative energy density, $E_{ac}/E_{ac,\,max}$, is displayed as a function of the coupling angle θ of the TA transducer for SF and FM actuation, respectively. Here, $E_{ac,\,max}$ represents maximum energy density measured by each active transducer (TA transducer active: 19.5 J m^{-3} at 75° and SF actuation; TA transducer passive: 3.53 J m^{-3} at 0° and SF actuation). Interestingly, averaged over all angles the energy densities are of similar magnitudes in both experiments. Thus, although
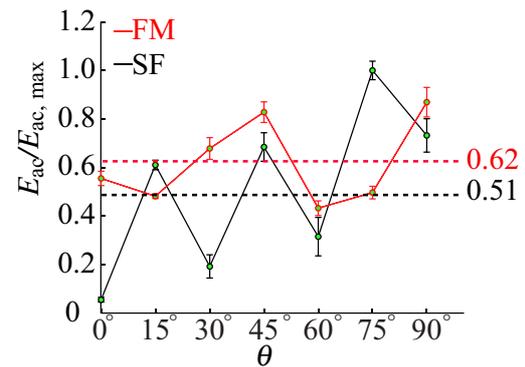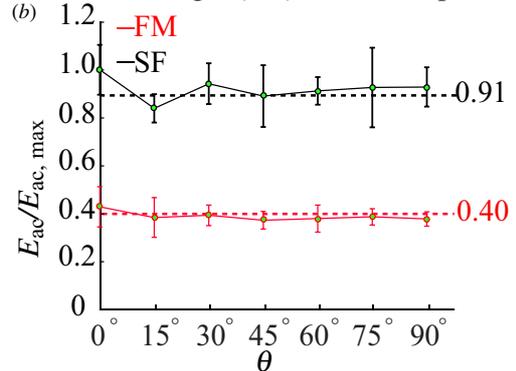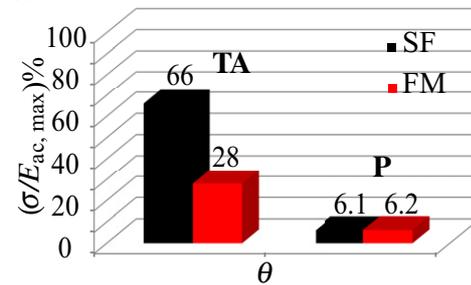

Figure 5. Relative energy density, $E_{ac}/E_{ac,\,max}$, as a function of the coupling angle θ of the (a) active and (b) passive TA transducer. (a): TA transducer active, driven at single frequency (SF, black line) and frequency modulation (FM, red line), and for (b): Planar (P) transducer active driven at single frequency (SF, black line) and frequency modulation (FM, red line), while changing the angle on the passive TA transducer. The values are normalized by the maximum value, $E_{ac,\,max}$, for each diagram, (a) and (b). The experiments were repeated four times for each angle and actuation method. (c): The normalized 1σ standard deviation ($\sigma/E_{ac,\,average}$) of the energy density values when changing the angle (from 0° to 90°) from the data displayed in (a) and (b).

we have not analyzed in detail all possible SFs within the FM bandwidth, we may conclude that FM actuation not only produces uniform particle patterns but also acoustic energy densities comparable to those produced with SF actuation. Still, the highest energy density noted was for SF (at the angle 75°.) Another interesting finding in figures 5(a) and (b) is the change in the energy density when varying the TA transducer angle. This is quantified in figure 5(c), where the 1σ standard deviation normalized by the average ($\sigma/E_{ac,\,mean}$)
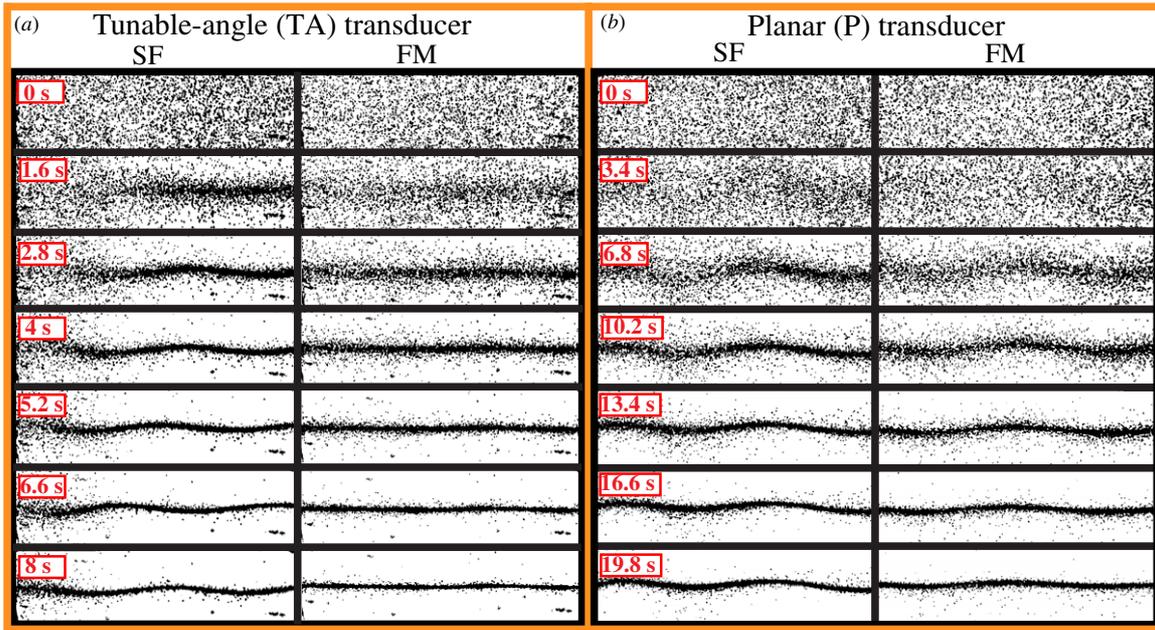
Figure 6. Dynamics of acoustophoresis patterns during (*a*): the first 8 s when actuating the device with the TA transducer and (*b*): the first 20 s when actuating the device with the planar (P) transducer. Both transducers were operated at $U_{pp} = 20$ V at single frequency (SF, left panel) and frequency modulation (FM, right panel). The angle of the passive TA transducer is fixed at 15°.
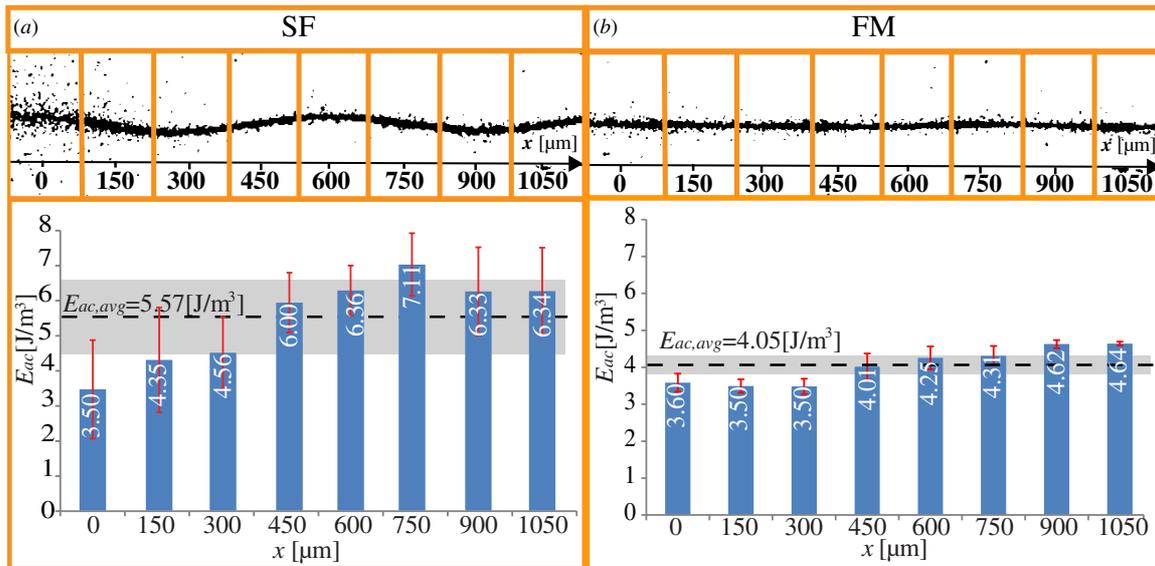

Figure 7. Measurement of the spatial distribution of the acoustic energy density along the micro-channel (*x*-axis), when actuating the chip with the TA transducer at (*a*) SF actuation, and (*b*) FM actuation. The light-intensity method was applied to eight 150 μm wide subsections of the recorded images. The angle θ of the TA transducer is fixed at 15°. The averaged energy density for the whole channel, $E_{ac, avg}$, is marked with a dotted black line, and the corresponding 1σ standard deviation is marked with a grey band. The red error bars are the standard deviations from the four repetitions of each experiment.

is displayed for the different actuation methods: TA active @ SF, TA active @ FM, TA passive and P active @ SF, TA passive and P active @ FM. As seen in the diagram, we note that the standard deviation is significantly higher for active TA transducer than for passive TA transducer. The highest standard deviation is noted for SF actuation of the active TA transducer. This suggests that the coupling angle has more effect than the transducer geometry change on the acoustic energy density.

4.2. Temporal and spatial effects of acoustophoresis

In order to investigate temporal effects as well as the spatial distribution in energy density for the different actuation approaches, we studied the dynamics of particle migration and pattern formation during acoustophoresis. This has previously been investigated in detail by Augustsson *et al* [16], but here we propose a less accurate but more simple method. For this analysis, we selected the coupling angle 15° since this angle
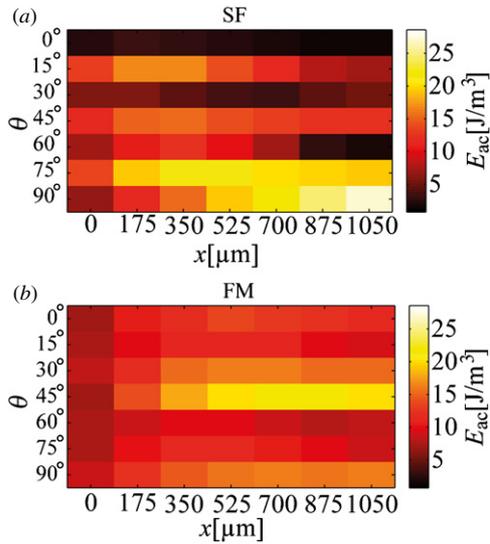
Figure 8. A 7 × 7 pixel color plot of the absolute energy density, E_{ac} as a function of the coupling angle (θ) and the position along the channel (x) when driving the chip with the TA transducer at SF actuation (*a*) and at FM actuation (*b*). The diagrams are based on 7 different wedge angles, 7 different channel positions (segments of length 90 μm) and 4 repetitions, i.e. 196 repetitions of the experiment in total. The overall variance (varying both θ and x) is three times higher for SF actuation than for FM actuation.

caused similar average acoustic energy densities for the two actuation methods (cf figure 5). The dynamics of the process was investigated for both SF and FM actuation, and for driving the system with either the TA transducer (figure 6(*a*)) or the P transducer (figure 6(*b*)) at $U_{pp} = 20$ V. As seen in the figures, the P-transducer acoustophoresis is weaker than TA-transducer acoustophoresis for the same driving voltage (approx. 2–3 times slower particle migration). However, this is primarily because of the use of a damping backing layer on the P transducer (this transducer was not optimized for achieving maximum energy density). More interestingly, the images clearly reveal the dynamics of acoustophoresis for the active TA transducer: for SF actuation, the particle migration is for this coupling angle locally faster in the right part of the images compared with FM actuation. However, FM shows a more uniform migration speed along the channel.

The correlation between the different migration speeds (cf figure 6) and acoustic energy density can be quantified with the light-intensity method. In figure 7, the light-intensity data from the experiment shown in figure 6(*a*) (TA transducer active) were used for calculating the spatial distribution in energy density along the channel. For this analysis, we divided the microscope images into eight segments. As seen in figure 7, the average energy density (dotted line) is similar for the two actuation approaches, but the variance along the channel is almost seven times larger for SF actuation (cf the standard deviation σ indicated by the gray band).

Finally, we quantified the spatial distribution of the energy density for all investigated wedge angles. The result is shown in figure 8 where the energy density is plotted versus both the wedge angle, θ, and the channel position, x. As can be seen in the diagram, both the overall variance as well as the local gradient in energy density is larger for SF actuation than for FM actuation (approx. three times higher variance for SF relative FM). Thus, together with figure 5 (where the spatial distribution is averaged out), figure 8 clearly confirms that the FM actuation method produces equally high but more uniform energy density than SF actuation in microchannel acoustophoresis.

4.3. Reproducibility

In order to confirm that the experimental data is reliable and consistent, reproducibility tests were performed for the TA transducer with the light-intensity model. These tests included mounting and demounting of the TA transducer between each experiment. Figure 9 shows the relative light intensities for three repetitions of the experiments for both SF and FM actuation. The data is taken from the same experiment as in figure 6, but here it represents the whole image width. In the diagram, the initial phase of particle migration toward the pressure node is marked with (I) and proceeds over approx. 10 s. This phase is used for the light-intensity model, and defines the acoustic energy density (cf equation (3)). The stationary phase is marked with (II), and is characterized with a much slower change in relative light intensity. However, it is interesting to see that although the change is slow, the relative light intensity is not constant in phase (II). One possible
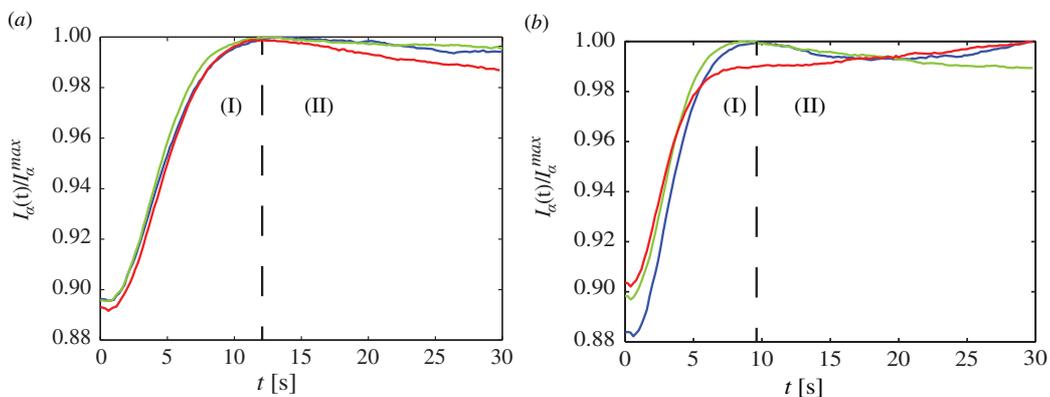
Figure 9. Reproducibility tests for the TA transducer, $\theta = 15°$. Normalized light-intensity curves $I_\alpha(t)/I_\alpha^{max}$ for (*a*) SF actuation, and (*b*) for FM actuation. Each experiment was repeated three times.

reason for this is that the acoustophoresis in our system is not 1D as assumed in the light-intensity model. Instead, 3D resonances and particle–particle interaction forces cause the formation of complex 3D patterns of agglomerated particles (cf figure 3). This can partly explain the negative slope in phase (II), e.g., when the pattern of agglomerated particles changes from straight to curved, and/or from a continuous line to a striated pattern. However, this effect is of less importance for the estimation of the acoustic energy density. Instead, in our light-intensity model the energy density is rather dependent on the slope of the relative light intensity during phase (I). In figure 9, the uncertainty of the experiments is 10 % for SF and 6 % for FM actuation. The lower uncertainty for FM actuation could be explained by the fact that the model is more applicable to 1D patterns.

5. Conclusions

We have analyzed the particle pattern and quantified the energy density of acoustophoresis in a microchannel when driving a microfluidic chip with a novel TA wedge transducer. Results were compared for two different actuation approaches: standard SF actuation, and our previously used actuation method based on repeating linear frequency sweeps, i.e., FM actuation. The particle pattern was analyzed by measuring the deviation from a straight line of focused particles as well as the variances in energy density along the channel and when changing the angle of the TA transducer. The energy density was measured by the use of a recently reported light-intensity method [18] applied to video recordings of particle migration during acoustophoresis. By comparing the results when tuning the angle of the active and passive TA-transducer (where for the passive case the chip was instead driven by a reference transducer of traditional P design), we conclude that the coupling angle is the more important parameter for controlling the acoustophoretic pattern at SF actuation with a wedge transducer, relative the transducer geometry. The most uniform pattern at SF actuation was obtained for coupling angles $\geqslant 75°$ for the TA transducer, i.e. when the coupling direction is close to parallel with the aimed force field inside the fluid channel. Furthermore, we conclude that FM actuation is not only robust and produces uniform particle patterns, but can result in average acoustic energy densities of comparable magnitudes to those obtained at SF actuation. Thus, FM actuation causes efficient and predictable acoustophoresis in a very straightforward manner, and reduces the need for calibration of the wedge angle. On the other hand, SF actuation with the active TA transducer could be used for fine-tuning of the shape of a complex resonance in the channel, but also for maximizing the acoustic energy density by tuning the angle into an optimal position. Even higher energy densities could be achieved with SF actuation if also the frequency is fine-tuned (which was not done in this study). This can be important for advanced acoustophoretic control in more complex channel structures actuated by several transducers and frequencies simultaneously [21, 22]. In such systems, the coupling angle may be used as an additional tuning parameter (to the standard tuning parameters which are the actuation frequency and the temperature) for controlling both the magnitude and spatial distribution of the resulting acoustic radiation force field when driving the device at single frequency.

References

[1] Bruus H, Dual J, Hawkes J, Hill M, Laurell T, Nilsson J, Radel S, Sadhal S and Wiklund M 2011 Forthcoming lab on a chip tutorial series on acoustofluidics. Acoustofluidics—exploiting ultrasonic standing wave forces and acoustic streaming in microfluidic systems for cell and particle manipulation *Lab Chip* **11** 3579–80

[2] Laurell T, Petersson F and Nilsson A 2007 Chip integrated strategies for acoustic separation and manipulation of cells and particles *Chem. Soc. Rev.* **36** 492–506

[3] Wang Z and Zhe J 2011 Recent advances in particle and droplet manipulation for lab-on-a-chip devices based on surface acoustic waves *Lab Chip* **11** 1280–5

[4] Haake A and Dual J 2004 Positioning of small particles by an ultrasound field excited by surface waves *Ultrasonics* **42** 75–80

[5] Manneberg O, Svennebring J, Hertz H M and Wiklund M 2008 Wedge transducer design for two-dimensional ultrasonic manipulation in a microfluidic chip *J. Micromech. Microeng.* **18** 095025

[6] Manneberg O, Vanherberghen B, Önfelt B and Wiklund M 2009 Flow-free transport of cells in microchannels by frequency-modulated ultrasound *Lab Chip* **9** 833–7

[7] Lenshof A, Evander M, Laurell T and Nilsson J 2012 Acoustofluidics 5: building microfluidic acoustic resonators *Lab Chip* **12** 684–95

[8] Hill M 2003 The selection of layer thicknesses to control acoustic radiation force profiles in layered resonators *J. Acoust. Soc. Am.* **114** 2654–61

[9] Bruus H 2012 Acoustofluidics 7: the acoustic radiation force on small particles *Lab Chip* **12** 1014–21

[10] Hagsäter S M, Lenshof A, Skafte-Pedersen P, Kutter J P, Laurell T and Bruus H 2008 Acoustic resonances in straight micro channels: beyond the 1D-approximation *Lab Chip* **8** 1178–84

[11] Manneberg O, Vanherberghen B, Svennebring J, Hertz H M, Önfelt B and Wiklund M 2008 A three-dimensional ultrasonic cage for characterization of individual cells *Appl. Phys. Lett.* **93** 063901

[12] Vanherberghen B, Manneberg O, Christakou A, Frisk T, Ohlin M, Hertz H M, Önfelt B and Wiklund M 2010 Ultrasound-controlled cell aggregation in a multi-well chip *Lab Chip* **10** 2727–32

[13] Christakou A E, Ohlin M, Vanherberghen B, Korshidi M A, Kadri N, Frisk T, Wiklund M and Önfelt B 2013 Live cell imaging in a micro-array of acoustic traps facilitates quantification of natural killer cell heterogeneity *Integr. Biol.* **5** 712–9

[14] Bazou D, Castro A and Hoyos M 2012 Controlled cell aggregation in a pulsed acoustic field *Ultrasonics* **52** 842–50

[15] Ohlin M, Christakou A E, Frisk T, Önfelt B and Wiklund M 2013 Influence of acoustic streaming on ultrasonic particle

manipulation in a 100-well ring-transducer microplate *J. Micromech. Microeng.* **23** 035008

[16] Augustsson P, Barnkob R, Wereley S T, Bruus H and Laurell T 2011 Automated and temperature-controlled micro-PIV measurements enabling long-term-stable microchannel acoustophoresis characterization *Lab Chip* **11** 4152–64

[17] Barnkob R, Augustsson P, Laurell T and Bruus H 2012 Acoustic radiation- and streaming-induced microparticle velocities determined by micro-PIV in an ultrasound symmetry plane *Phys. Rev.* E **86** 056307

[18] Barnkob R, Iranmanesh I, Wiklund M and Bruus H 2012 Measuring acoustic energy density in microchannel acoustophoresis using a simple and rapid light-intensity method *Lab Chip* **12** 2337–44

[19] Barnkob R, Augustsson P, Laurell T and Bruus H 2010 Measuring the local pressure amplitude in microchannel acoustophoresis *Lab Chip* **10** 563–70

[20] Yosioka K and Kawasima Y 1955 Acoustic radiation pressure on a compressible sphere *Acoustica* **5** 167–73

[21] Svennebring J, Manneberg O, Skafte-Pedersen P, Bruus H and Wiklund M 2009 Selective bioparticle retention and characterization in a chip-integrated confocal ultrasonic cavity *Biotechnol. Bioeng.* **103** 323–32

[22] Manneberg O, Hagsäter S M, Svennebring J, Hertz H M, Kutter J P, Bruus H and Wiklund M 2009 Spatial confinement of ultrasonic force fields in microfluidic channels *Ultrasonics* **49** 112–9